Hindawi
Journal of Nanomaterials
Volume 2023, Article ID 8825762, 10 pages
https://doi.org/10.1155/2023/8825762

Research Article

ZnO Nanoparticles Synthesized using Aerial Extract of *Ranunculus multifidus* Plant: Antibacterial and Antioxidant Activity

Terfo Yilma,[1] **Mikyas Kassaw**,[1] **H. C. Ananda Murthy**,[1,2] **and Aman Dekebo**[1,3]

[1]*Department of Applied Chemistry, School of Applied Natural Science, Adama Science and Technology University, Adama P.O. Box 1888, Ethiopia*
[2]*Department of Prosthodontics, Saveetha Dental College and Hospital, Saveetha Institute of Medical and Technical Science (SIMATS), Saveetha University, Chennai 600077, Tamil Nadu, India*
[3]*Institute of Pharmaceutical Sciences, Adama Science and Technology University, Adama P.O. Box 1888, Ethiopia*

Correspondence should be addressed to H. C. Ananda Murthy; anandkps350@gmail.com and Aman Dekebo; amandekeb@gmail.com

Received 28 December 2022; Revised 8 February 2023; Accepted 25 April 2023; Published 21 May 2023

Academic Editor: Jagpreet Singh

The present work reports the synthesis of zinc oxide nanoparticles (ZnO NPs) by applying an aqueous aerial extract of *Ranunculus multifidus* plant. The thermogravimetric analysis revealed that the prepared ZnO NPs are stable from 480 to 800°C. The diffraction study confirmed the hexagonal wurtzite structure for the synthesized ZnO NPs with the typical crystallite sizes of 47.92, 22.70, and 15.35 nm the volume ratios (extract to precursor) of 1 : 1, 3 : 2, and 2 : 3, respectively. The experimentally deduced E_g values are 1.82, 3.1, and 2.57 eV for 1 : 1, 3 : 2, and 2 : 3 ZnO NPs, respectively. The spherical and rod-like morphologies were confirmed for the NPs by the images taken using electron microscopy. The reducing agents in the aqueous extracts of *R. multifidus* converted the ionic zinc to zinc nanoparticles, and these NPs exhibit credible antibacterial effects against tested bacterial species. The biosynthesized ZnO NPs revealed significant antibacterial activity against *Bacillus subtilis*, *Escherichia coli*, *Pseudomonas aeruginosa*, and *Staphylococcus aureus*. The order of the antibacterial potential of the NPs was found to follow the order: *S. aureus* (17.10 ± 0.45 mm) > *B. subtilis* (16.10 ± 0.15 mm) > *E. coli* (14.5 ± 0.32 mm) > *P. aeruginosa* (13 ± 0.0 mm). The antioxidant activities of the produced ZnO NPs in various ratios showed the potentiality of phytochemicals to scavenge the free radicals, which is encouraging for the discovery of novel compounds for the treatment of cancer diseases.

1. Introduction

The novel method of plant-mediated synthesis of nanoparticles (NPs) has numerous applications in medicine, pharmacy, industry, and agriculture. Due to their toxicity, conventionally produced NPs are only occasionally used in the therapeutic setting. We are currently observing the growth and development of a new interdisciplinary scientific discipline called nanoscience [1–8]. There are many methods for the production of nanoparticles, but green synthesis is one of the most popular since it is safe for the environment, nontoxic, cheap, and extremely pure. A chemical wet method was also used to prepare nanomaterial, especially with ZnO–Ag and ZnO–Au as nanocomposite materials by using the precipitate method [9]. Noble metal and metal oxide nanoparticles including silver, copper, gold, platinum, CuO, and Ag_2O were produced using many plant extracts by adopting the green methodology. But among many metal oxide NPs, zinc oxide nanoparticles (ZnO NPs) shine in the biological and pharmaceutical industries.

In recent years, different industrial sectors, such as pharmaceuticals, cosmetic, and concrete industries, have begun to use zinc oxide as some key ceramic materials instead of the microbiological, textile, and automotive industries. Due to the worrisome rise in the incidence of bacterial infectious illnesses and their resistance to most first-line antibiotic agents, antibacterial therapy has proven challenging [10].

In the twenty-first century, this poses a serious risk to human health, necessitating urgently continuing research to find agents with stronger antibacterial and broad-spectrum activities.

Therefore, finding novel drugs to treat disease and inflammations without causing significant negative impacts on patients was the current project on which all researchers were engaged. In nanoscale formulations, ZnO NPs are now being studied as potential allies of antioxidant and antibacterial medicines. The ZnO NPs have anticancer properties and are frequently used to treat a variety of skin problems [6]. Furthermore, ZnO NPs have been used as a recent preferable tool in drug delivery and sensing horizons. Traditional medicines in a different country have a long history and are mostly based on rich, though unstandardized, pharmacopeia made primarily from plants that are used by patients at home for self-administration as well as traditional healers [11]. Due to its ethnomedicinal benefits that have been reported in various locations by different herbalists and researchers, *Ranunculus multifidus*, one of the traditional medicinal plants primarily found in Africa, particularly Ethiopia, is taken into consideration in this work [12]. The bio-diversified species of flowering plant *R. multifidus*, often known as buttercup in South Africa, belongs to the *Ranunculaceae* family. With the exception of West Africa, Madagascar, and the Arabian Peninsula; it is indigenous to Sub-Saharan Africa [12]. Anti-rheumatism, intermittent fever, and rubefacient are the three traditional uses of *Ranunculus* species [13]. In a similar situation, *R. multifidus* was also traditionally used to cure several diseases. The most widely adopted traditional uses includes treatment of TB [14], infertility, blood cleansing [15], eye infection [16], shingles and sores, malaria [17], and others. This traditional use of the plant might emanate from its phytochemical components such as flavonoids, saponins, alkaloids, glycosides, terpenoids, anthocyanins, and quinones. Despite the plants having a wide range of conventional applications, there are no reports of this amazing herb being used to synthesize nanoscale materials. The main objective of the current study was to explore or search the application of *R. multifidus* plant aerial extract as a capping and reducing agent for the synthesis of ZnO NPs because it is a rich source of bioactive compounds and investigate their antibacterial and antioxidant activity in light of the significance of green nanoparticles and research gap toward the plant mentioned. The plant extract transforms ionic zinc to metal zinc oxide nanoparticles by acting as a reducing and capping agent. Therefore, the antibacterial activity of synthesized ZnO NPs was evaluated against Gram-negative and Gram-positive bacterial strains namely, *Escherichia coli*, *Pseudomonas aeruginosa*, *Staphylococcus aureus*, and *Bacillus subtilis*. In addition, the radical scavenging activities of synthesized NPs were evaluated using the DPPH methods. The result of the present work revealed that the synthesized nanoparticles exhibited significant antibacterial activities, especially on Gram-positive pathogenic strains. The radical scavenging activities of ZnO NPs are promising for the disease-associated ROS. To the best of our knowledge, this research was the first and novel work using this plant and gives a great clue for further works, especially using nanohybrid materials to enhance the potency of nanoparticles for different biomedical applications.

2. Materials and Methods

2.1. Plant Material Collection and Identification. The aerial parts of the plant *R. multifidus* were picked from Bekoji, Oromia region, Arsi zone. The authentication of the plant was done at the National Herbarium of Ethiopia, Addis Ababa University (voucher no. TY-001).

2.2. Preparation of Plant Extracts (Broth Solution). R. multifidus fresh plant material was collected, completely cleaned with distilled and tap water to get rid of the dust, and then dried in the shade to get rid of any remaining moisture. The powdered plant materials were sieved using 180 m size sieves after being pounded into powder. The sample's aqueous extracts were made by boiling 50 g of finely ground powder for 60 min at 80°C with constant stirring. After filtering the extract using Whatman no. 1 filter paper and allowing it to cool to room temperature, the extract was kept in a refrigerator at 4°C for future experimental usage [5].

2.3. Synthesis of ZnO NPs. Three different ratios *R. multifidus* plant extract and precursor salts were used: 1 : 1, 3 : 2, and 2 : 3, 50 mL, 60 mL, 40 mL of extract and 50 mL, 40 mL, and 60 mL of 0.2 M zinc acetate ($Zn(O_2CCH_3)_2(H_2O)_2$), were mixed with 50 mL of 0.2 M NaOH, respectively.

A yellow precipitate formed after the three solutions were continuously for 2 hr at 800 rpm using a magnetic stirrer [18]. The precipitate was periodically cleaned in ethanol and distilled water to get rid of any impurities left behind, and they were then oven dried at 100°C for an hour. Using a blender, the produced dried light yellow color powder was prepared for further characterization and applications. The overall synthesis process was depicted in Figure 1.

2.4. Characterization of Biosynthesized ZnO NPs. A simultaneous DTA-TGA (DTG-60H, Shimadzu Co., Japan) study was used to examine the thermal stability and decomposition followed by the weight loss of the prepared ZnO NPs measured at the heating rate of 10°C/min. An ultraviolet–visible (UV–vis) spectrophotometer was utilized to identify the surface plasmon resonance (SPR) peak. Using Fourier transform infrared spectroscopy, the potential phytochemicals causing the reduction of metal salts into ZnO NPs were examined (FTIR). The external morphology, surface features, and elemental compositions of ZnO NPs were analyzed using -microscopic methods combined with energy-dispersive X-ray analysis (SEM-EDX).

2.5. Antibacterial Investigation of Synthesized ZnO NPs. The antibacterial activity of biosynthesized ZnO NPs was performed using the agar disc diffusion method against human infectious, *B. subtilis*, *E. coli*, *P. aeruginosa*, *and S. aureus*, bacterial strains which were American Type Culture Collection (ATCC). In nutrient broth, cultures of the test organism were grown to the late logarithmic phase. Aliquots of 100 μL from the cultures were spread on solidified nutrient agar plates. The plates were coated with the 100 μL solution of 50, 75, and 100 μg/mL concentration of ZnO NPs solution impregnated disc (6 mm). The plates were then placed upside down in the incubator at 37°C for 24 hr. To ensure that bacterial cells and agar were mixed equally, the plates were gently shaken. After

Figure 1: A schematic of the synthesis of ZnO NPs using *Ranunculus multifidus* plant extract.

the incubation period got over, different levels of zonation formed around the disc were measured using a caliper. This procedure was done for all ratios of biosynthesized ZnO NPs against standard bacterial strains.

2.6. DPPH Radical Scavenging Assay. DPPH radical scavenging assay was conducted according to the previously described standards with little modification, the DPPH test was used to evaluate the free radical scavenging activity (RSA) of the plant extract and synthesized ZnO NPs of various ratios (1 : 1, 2 : 3, and 3 : 2) salt to plant aqueous aerial extract [19]. The 1,1-diphenyl-2-picryl hydrazyl (DPPH), a persistent free radical, can decolorize in the presence of antioxidants, which is the basis for the DPPH antioxidant assay. The odd electron in the DPPH radicals is what causes the absorbance at 517 nm as well as the apparent to deep purple color. A decrease in the absorbance of the reaction mixture indicates significant free radical scavenging activity of the extract or synthesized NPs. The data were compared with those obtained with the reference ascorbic acid. In the process, the synthesized ZnO NPs of different ratios (1 : 1, 2 : 3 and 3 : 2) salt to plant extract ration were dissolved in methanol to afford 1 mg/mL. It was serially diluted in methanol to yield a 500, 250, 125, and 62.5 μg/mL concentration. Four milliliters of DPPH (0.004% DPPH in MeOH) was added to 1 mL of each concentration to make 100, 50, 25, and 12 μg/mL. Then all the samples prepared were incubated in an oven at 37°C for 30 min and then absorbance was recorded at 517 nm using a UV–vis spectrophotometer. A reaction solution without DPPH was used as blank and DPPH solution as a control. Ascorbic acid was used as standard. The percentage inhibition was calculated using the Equation (1):

$$\text{Inhibition } (\%) = \frac{\text{A control} - \text{A test}}{\text{A control}} \times 100. \quad (1)$$

The IC_{50}, or the concentration of the test substance needed to cause a 50% reduction in absorbance from that of the control solution, is another way to express the sample's ability to scavenge DPPH radicals [20]. The concentration vs. RSA% graph was produced using Excel, and the IC_{50} values were calculated from it and interpreted as the smallest IC_{50} values mean the strongest radical scavenging concentration of extracts.

3. Results and Discussion

3.1. Synthesis ZNO NPs. Using *R. multifidus* and zinc acetate dihydrate salt as a precursor, ZnO NPs were synthesized. The aerial extract from *R. multifidus* was used as a reducing and capping agent. The presence of flavonoids, phenolic compounds, tannins, saponins, anthraquinone glycosides, reducing sugars, phytosterols, steroids, terpenoids, and glycosides in the plant extracts revealed the phytochemical screening of the extracts. The information on the phytochemicals in the extract is provided in Table 1. The three main processes that go into making NPs, metal ion reduction, cluster formation, and nanoparticle development, are thought to be extremely important. The tautomeric conversion of polyphenols from

Table 1: The result of the phytochemical screening of the aerial extract of the *R. multifidus* plant.

No.	Phytochemicals	Test types/reagent	Result
1	Flavonoids	Shinoda Test	+
2	Saponins	Foam test	+
3	Phenol	Ferric chloride test	+
4	Cardiac glycosides	Keller–Killiani Test	+
5	Terpenoids	Salkowski Test	+
6	Reducing sugars	Fehling's test	–
7	Phytosterols	Salkowski Test	+
8	Tannins	Alkaline test	–
9	Anthraquinone glycosides	Borntrager's Test	+
10	Steroids	–	+
11	Alkaloids	Wagner's test	–

NB: + indicates the presence and – indicates the absence.

their enol form to their keto form can be expected to reduce the zinc ions to zinc NPs.

Additionally, the enzymes in the aerial extract of the plant assist the metal ions to create an enzyme–substrate complex, which results in the production of zinc with a protein cap [21], and it is known that the phenolic chemicals serve as ligands, bind to metal ions, decrease, and cap those ions to create nanoparticles. A prior study had also claimed that these ligands also function as regulators of particle size [21, 22]. The great propensity of phenolic compounds to chelate metals is the main cause of their antioxidant function. The hydroxyl and carboxylic groups found in phenolic compounds have a very high propensity to attract metal ions. In solution, the phenolic chemicals interact with metal ions, assisting in the nucleation and production of ZnO NPs.

3.2. Characterization of Synthesized ZnO NPs. The synthesized ZnO NPs were characterized by using the TGA and its derivative (DTA), UV–vis-DRS, FT-IR, XRD, and SEM techniques.

3.2.1. Thermogravimetric Analysis (TGA) and Its Derivative (DTA). The sample's mass loss is shown by the TGA curve, while the process's energy gain or loss is shown by the DTA curve [5]. Figure 2 depicts the thermal analysis plots of the uncalcined ZnO NPs (1 : 1).

The three primary steps were observed from the ZnO NPs TGA curves; 6.89% of the water molecules in the first curve, in the temperature range from 20 to 250°C, reveal the dehydration of adsorbed water. In the second breakdown loss, which occurs as the temperature rises from 240 to 480°C, 10.75% of Zn $(OH)_2$ transforms into ZnO NPs. The remaining decomposition losses from 480 to 800°C are not displayed in the third stage. According to the evidence of breakdown losses, residual surfactants, or steady heat follow, ZnO NPs were found to be thermally stable from 480 to 800°C. The outcome of this investigation was consistent with earlier published research [23]. As a result, for all other manufactured ZnO NPs throughout this experiment, calcination temperatures of up to 480°C were used.

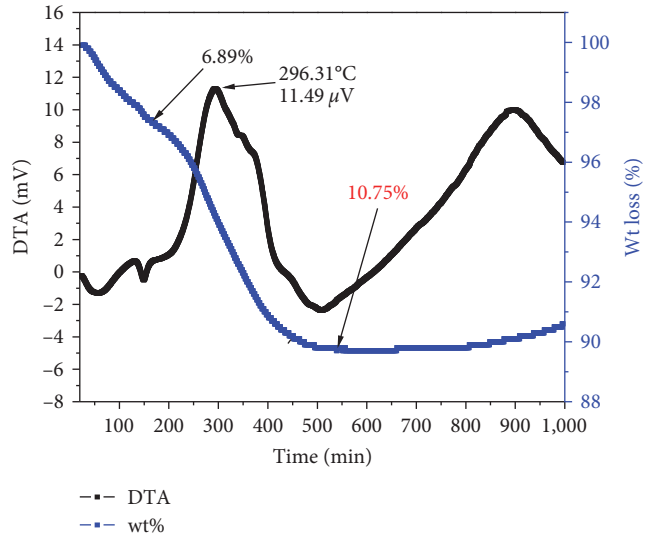

Figure 2: Thermal analysis plots of ZnO NPs obtained using the aerial extract of *Ranunculus multifidus* plant.

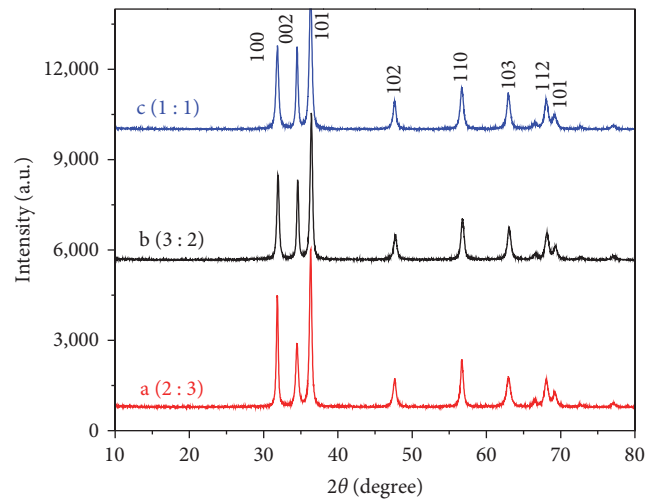

Figure 3: XRD patterns of the synthesized ZnO NPs with different ratios: (a) 2 : 3, (b) 3 : 2, and (c) 1 : 1.

3.2.2. XRD Analysis. X-ray diffraction technique was utilized to explore the structure and crystallite size of the synthesized ZnO NPs. Figure 3 displays the diffraction pattern of ZnO NPs made from zinc acetate precursor and *R. multifidus* plant aerial extract in three different volume ratios, such as (1 : 1), (2 : 3), and (3 : 2). The lattice planes (100), (002), (101), (102), (110), (103), and (112) are successively represented by the 2θ values, 32.01°, 34.50°, 36.25°, 47.71°, 56.71°, and 68.00° in the XRD analysis of ZnO NPs. All the diffraction peaks recorded for the NPs were discovered to be in compliance with the literature report [5, 23]. The findings support the synthesis of pure ZnO NPs without the creation of any secondary phase and are in good accord with Miller index values and the hexagonal wurtzite structure of ZnO (JCPDS card no. 036-145). The evaluation using Scherer's formula (Equation (2)) revealed the typical crystallite size of 47.92,

Table 2: The parameters obtained from the diffraction studies for the ZnO NPs synthesized using 1 : 1, 3 : 2, and 2 : 3 rations of the salt to extract.

Ratios of ZnO NPs	2θ (degree)	FWHM (θ)	FWHM (3.14/180)	hkl	D	D_{av} (nm)
	33.3608	0.17470	0.003049	100	49.5813	
1 : 1	35.8293	0.18160	0.00317	102	48.01849	47.92
	54.2561	0.20190	0.003524	101	46.1763	
	36.8235	0.48210	0.008424	100	18.1394	
3 : 2	15.9989	0.27670	0.004929	102	30.2815	22.70
	65.1727	0.50000	0.008727	101	19.6951	
	36.8697	0.58190	0.010156	100	15.0304	
2 : 3	65.2310	0.63670	0.011113	102	15.4716	15.35
	59.3379	0.61330	0.010704	101	15.57032	

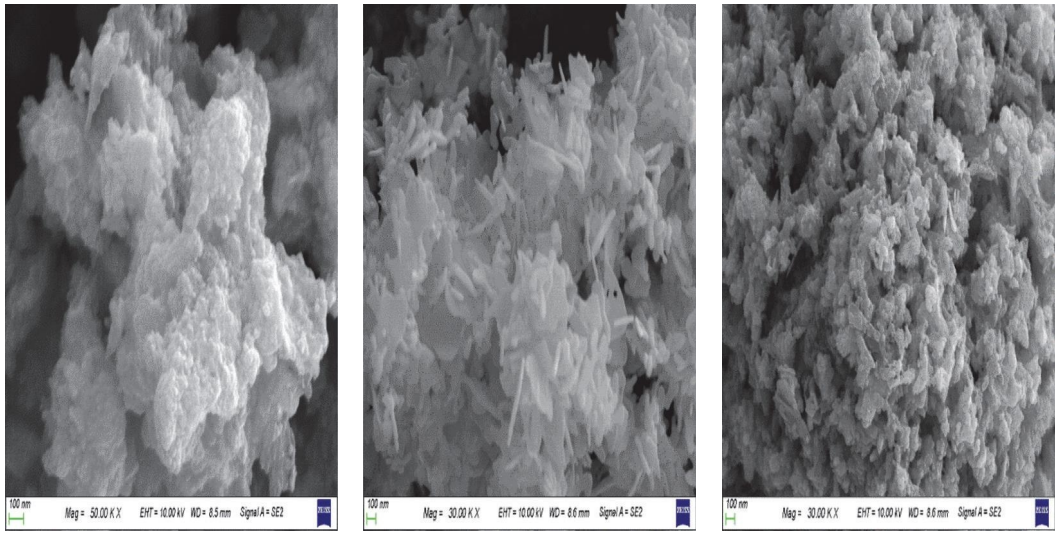

(a) (b) (c)

Figure 4: SEM images of (a) 1 : 1 ZnO, (b) 3 : 2 ZnO, and (c) 2 : 3 ZnO NPs.

22.70, and 15.35 nm for ZnO NPs prepared in the volume ratios of (1 : 1), (3 : 2), and (2 : 3), respectively.

$$D = \frac{K}{B \cos \theta}, \tag{2}$$

where D is the crystallite size, K is 0.9 diffraction constant (shape factor), λ is 1.54 (X-ray source wavelength), β is the full width at half maximum intensity (FWHM) in radians, and θ is the angle of diffraction.

Table 2 displays the estimated and measured XRD parameters for crystallite size. The calculated and measured crystallite size XRD characteristics are shown in Table 2. The results revealed that the ratio of the plant extract grew from 1 : 1 (47.92 nm) to 3 : 2 (22.7 nm) and to 2 : 3 (15.35 nm) volume ratios, the average crystal size of ZnO NPs were found to increase. Since a greater amount of the plant extract was used during the synthesis process, it results in effective capping and stabilization of the synthesized nanoparticles and hinders the process of aggregation. This precisely matches the previously stated method of the production of ZnO NPs [24].

3.2.3. SEM Analysis. SEM was used to examine the surface morphological characteristics of the ZnO NPs. The micrographs are presented in Figure 4(a)–4(c). Figure 4(a) displays a micrograph of ZnO NPs produced using a 1 : 1 volume ratio of plant aerial extract and zinc acetate salt. ZnO NPs with a 1 : 1 volume ratio appeared as a honeycomb-like structure in the SEM picture. The increase of the nanoparticles' size and the accumulation of zinc acetate and plant extract on their surface are what caused it to occur. Due to the increased concentration of zinc ions followed by aggregation on the surface for ZnO NPs in 3 : 2 volume ratios resulted in a road-like form and the ZnO NPs with 2 : 3 volume ratio, exhibited a spherical form [25]. According to the current work and earlier literature findings, the ability of the extract to serve as a cap during the nucleation, aggregation, and formation of NPs was what caused the reduction in size upon increasing plant extract concentration [25].

3.2.4. Fourier Transform Infrared (FTIR) Analysis. Figure 5 shows the FTIR spectra of ZnO NPs and aerial extract of *R. multifidus* plant. Biomolecules were found in the extract and NPs by FTIR spectral analysis. The major peaks that were

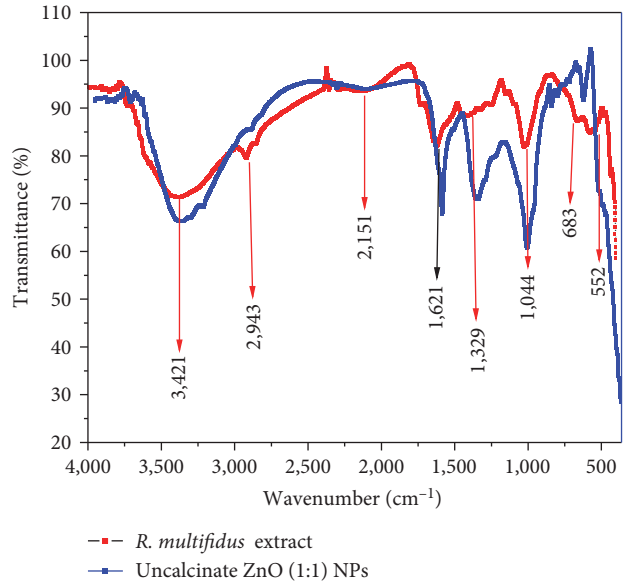

Figure 5: FTIR spectra of *Ranunculus multifidus* plant extract and synthesized ZnO NPs (1 : 1).

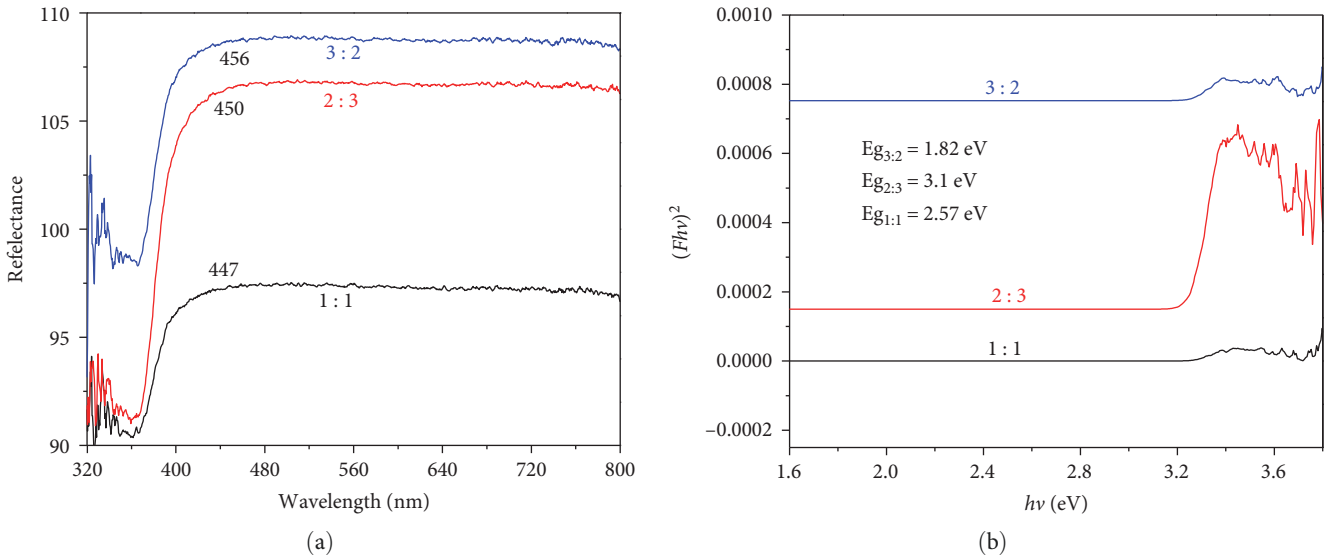

Figure 6: (a) UV–visible reflectance spectra, and (b) band gap energy of ZnO NPs.

detected at 3,421 and 2,943 cm^{-1} represent, sp^3 C–H stretching vibrations and the OH stretching vibration of carboxylic acid, respectively. The vibration of the CN moiety from the protein molecule of the extract is responsible for the peak at 2,151 cm^{-1}. The peak at 1,621 cm^{-1} is related to carbonyl groups that have undergone C=O stretching and may be acidic carbonyl groups. Sharp peaks around 1,329 cm^{-1} indicate the existence of the carboxylic acid COO– group. Additionally, it was demonstrated that the amine and carboxylate groups in the *R. multifidus* aerial extract were in charge of adhering to the surface of ZnO and stabilizing the biosynthesized ZnO NPs as well as fitting the prior literature study [21]. Around 1,044 cm^{-1}, the C–O–C stretching becomes visible. The peak at around 552 cm^{-1} can be attributed to the stretching vibration of the Zn–O bond. The bending vibrations of Zn–O–H bonds resulted in a tiny peak at 683 cm^{-1}.

3.2.5. UV–Vis–DRS Spectral Analysis. Diffuse reflectance spectroscopy (DRS) was used to assess the optical energy band gap (E_g) values of the synthesized ZnO NPs in volume ratios (1 : 1, 2 : 3, and 3 : 2) as shown in Figure 6. The sample's reflectance spectrum was found to be highly reflective between 447 and 456 nm in the UV spectrum, attaining a practically constant value thereafter, and the results were consistent with the report [26, 27]. The Kubelka–Munk formula (Equation (3)) was applied to convert the measured reflectance to absorbance.

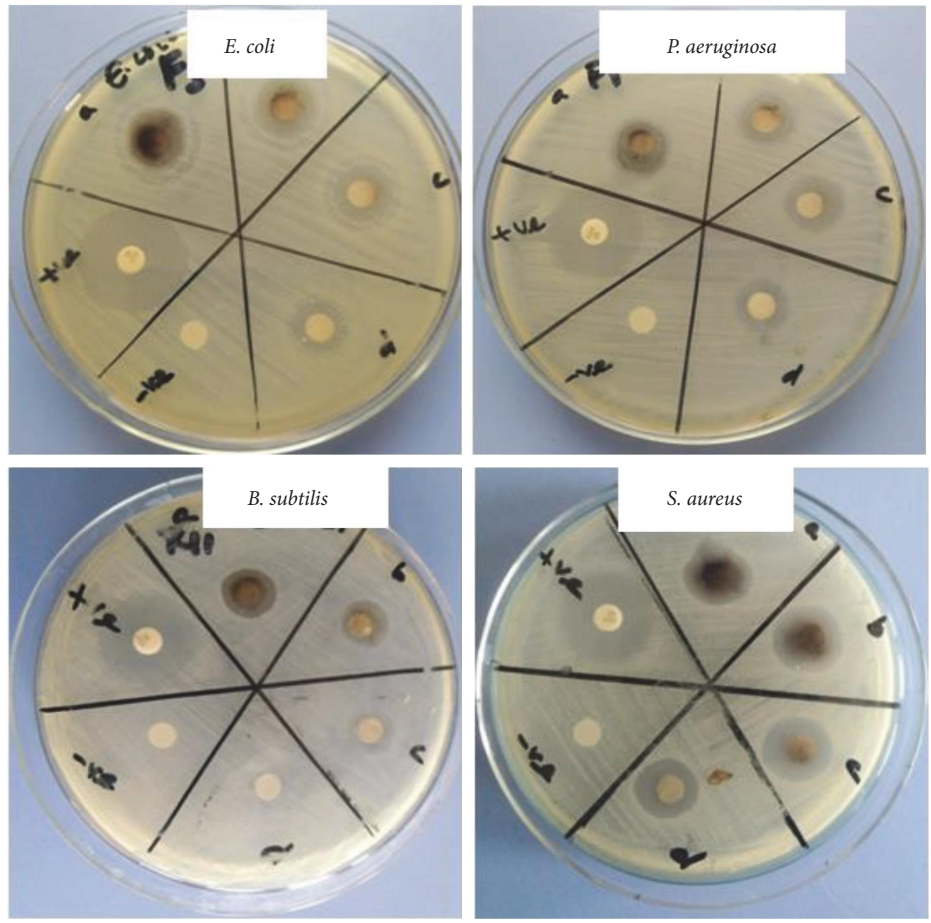

Figure 7: Inhibition zone of bacterial strain using disc diffusion methods using 2 : 3 ratio of ZnO NPs sample.

$$F(R)h\nu = A\left(h\nu - E_g\right)^n, \tag{3}$$

where A is the transition probability, $h\nu$ is photon energy and the exponent factor, n is the nature of the optical transition (n can take up the values ½ or 2).

The bandgap energies (E_g) of synthesized ZnO NPs with the volume ratios of (1 : 1), (2 : 3), and (3 : 2) were 1.82, 3.1, and 2.57 eV, respectively, and were calculated based on Equation (3); the fraction of reflectance (F), the photon energy ($h\nu$), and direct bandgap energies (E_g). ZnO (2 : 3) NPs have a higher E_g value than the other two volume ratios. On the other hand, the 2 : 3 ratio's average crystallite size from XRD shows that it is smaller than the other counterpart. As the concentration of the extract increases, the increased concentration of the phytochemicals stabilizes small particles by effectively capping them. This intern accounts for the decreased aggregation effect. If the particle size is very small, light interacts with the samples instead of being absorbed by it, with some of the light being reflected and scattered. This intern demonstrates the prior report's finding that the band gap energy of greenly produced ZnO NPs has an inverse relationship with the average crystalline size [27].

3.3. Antibacterial Activity. *S. aureus*, *B. subtilis*, *E. coli*, and *P. aeruginosa* were all tested pathogens, and the ZnO NPs have exhibited a wide spectrum of antibacterial activity against all of them. This study evaluated how biomolecules and ZnO NPs worked together to combat four pathogenic diseases. Three concentrations of Co-clotrimazole, DMSO, and ZnO NPs (50, 75, and 100 μg/mL) were used to determine the zone of inhibition. The structural differences in bacteria cell walls are assumed to be the reason why ZnO NPs were discovered to have superior antibacterial action against Gram-positive bacteria than Gram-negative bacteria [5, 21]. The outer lipopolysaccharide membrane of Gram-negative bacteria, which renders the cell wall resistant to antibacterial chemical substances, is the source of these variances in morphological constitutions between these micro-organisms. Gram-positive bacteria, on the other hand, are more prone to permeability barriers since they only have an exterior peptidoglycan layer. Due to their more intricate cell walls than Gram-positive bacteria, Gram-negative bacteria are less susceptible to antibacterial medications and act as a diffusion barrier. The presence of bioactive chemicals that functions as capping and stabilizing agents on the surface of NPs can be partially blamed for the antibacterial activities of NPs. The ZnO NPs exhibited excellent antibacterial activity against both Gram-positive (*S. aureus* and *B. subtilus*) and Gram-negative (*E. coli* and *P. aeruginosa*) bacterial strains, as shown in Figure 7 (Table 3). When we compared the inhibition zone for each

Table 3: Zone of inhibition (mm) of ZnO nanoparticles against Gram positive and Gram-negative bacterial strains.

Ratios	Conc. (μg/mL)	Bacteria species and zone of inhibitions in mm			
		E. coli ATCC 25922	*S. aureus* ATCC25923	*P. aeruginosa* ATCC27853	*B. subtilis* ATCC6633
1 : 1 ZnO	a 50	6 ± 1.12	7.5 ± 0.56	5.5 ± 0.32	8.24 ± 0.30
	b 75	7.8 ± 0.76	9.8 ± 0.48	6.32 ± 0.25	9.5 ± 0.73
	c 100	10.7 ± 0.45	13.85 ± 0.44	9.3 ± 0.78	12.9 ± 0.18
2 : 3 ZnO	a 50	10 ± 0.67	12.7 ± 0.25	9.2 ± 0.36	12 ± 0.54
	b 75	12.8 ± 0.40	14.9 ± 0.65	11.7 ± 0.65	14 ± 0.50
	c 100	14.5 ± 0.32	17.10 ± 0.45	13 ± 0.0	16.10 ± 0.15
3 : 2 ZnO	a 50	8 ± 0.00	10 ± 0.52	8.2 ± 0.41	9 ± 0.74
	b 75	11 ± 0.50	11.5 ± 0.32	9.0 ± 0.55	11.34 ± 0.5
	c 100	$13.72.10 \pm 0.24$	14 ± 0.65	12.45 ± 0.82	14.53 ± 0.32
Standard	Co-clotrimazole	22.5 ± 0.27	25 ± 0.55	22 ± 0.42	24 ± 0.15

Table 4: % radical scavenging activity of the ZnO NPs.

Conc. (μg/mL)	Absorbance of sample				DPPH (%) inhibition			
	P_1M_1	P_2M_3	P_3M_2	AA	P_1M_1	P_2M_3	P_3M_2	AA
12.5	0.47	0.36	0.25	0.02	48.85	60.82	72.80	98.44
25	0.42	0.31	0.21	0.01	54.23	66.26	77.14	98.5
50	0.38	0.28	0.18	0.013	58.64	69.53	80.41	98.54
100	0.32	0.25	0.15	0.012	65.18	72.79	83.67	98.59
Control 0.9188								

P, plants extracts, *M*, metal ions; AA, ascorbic acid; the number stands for volume of ratios.

ratio of biosynthesized NPs, the maximum inhibition was seen for (2 : 3) ZnO NPs for each strain. This could be a result of the synergistic effects of phytochemicals included in plant extracts as well as the propensity of functional groups like phenolics and amines to interact with metal surfaces and disturb membrane integrity. At a sample concentration of 100 μg/mL, the inhibition zone for each strain is displayed in descending order for this maximum ratio; *S. aureus* (17.10 ± 0.45 mm), *B. subtilus* (16.10 ± 0.15 mm), *E. coli* (14.5 ± 0.32 mm), *P. aeruginosa* (13 ± 0.0 mm); the NPs with a 1 : 1 ratio showed lesser inhibition [24]. The alternative explanation could be that Zn antimicrobial activities are owing to its toxicity, which was noted in this experimental study and other similar works that have previously reported on the antimicrobial properties of this metal-based NPs [24, 28].

The inhibition zone of each strain was concentration-dependent, which is explained by the linear association between NPs concentration and the inhibitory effect, according to the table of antibacterial activity results. Scientists have proposed a few potential bactericidal pathways in response to ZnO NPs' interactions with bacteria. Some researchers asserted that because smaller NPs have more surface reactivity, the released Zn^{2+} ions can penetrate them more deeply. One of the most popular theories for an antibacterial mechanism involves the release of Zn^{2+} from ZnO NPs, which is known to block several bacterial cell functions, including active transport, bacterial metabolism, and enzyme activity. Because of the toxicity properties of Zn^{2+}, this ultimately causes bacteria to perish [28–32].

Some other researchers made the hypothesis that the production of reactive oxygen species (ROS), which results in oxidative stress and, ultimately, cell damage or death, is what triggers antibacterial action. ZnO NPs frequently use the generation of ROS as an antibacterial strategy [5, 24]. The attachment of NPs to the bacterial cell membrane by electrostatic forces is another potential mechanism for the antibacterial activity of ZnO NPs. This interaction could harm the bacterial cell's integrity and alter the membrane plasma structure, allowing internal contents to seep out and ultimately leading to cell death [8, 21].

3.4. DPPH Radical Scavenging Assay. The synthesized ZnO NPs demonstrated the presence of antioxidant capabilities in an *in vitro* antioxidant experiment. The relationship between different volume ratios of synthetic ZnO NPs produced from aerial extracts and their capacity to scavenge DPPH radicals was proven (Table 4). All the antioxidant models showed a percentage of inhibitions, indicating that the produced ZnO NPs were effective at scavenging free radicals up to the specific concentration (Figure 8). According to the results in Table 4, the synthesized NPs have a negligible antioxidant effect in comparison to the reference standard.

P_3M_2 had the highest level of radical inhibition values of 83.67% at maximum concentration (100 μg/mL), which was comparable to L-ascorbic acid at this concentration when comparing the radical scavenging capability of various ratios. The P_2M_3 test yielded results that were second-most promising, with antiradical inhibition effects (100 μg/mL) of

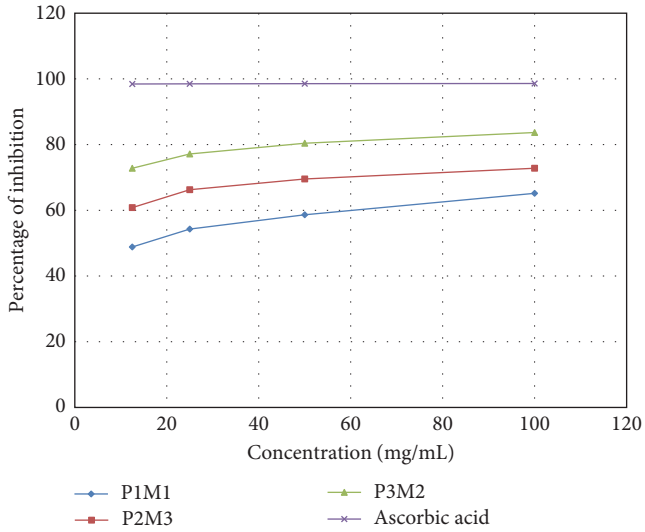

FIGURE 8: Graphical representation of radical scavenging power of synthesized ZnO NPs using different volume ratios of plant extracts to metal.

72.79% compared with L-ascorbic acid, which inhibited at a rate of 98.59% at the same concentration (Table 4). Overall, the results demonstrate that the synthetic zinc oxide nanoparticles generated from *R. multifidus* aerial extracts offer a useful lead for future research into the development of antioxidant drugs to treat various cardiovascular diseases using more sophisticated instrumentation and cutting-edge technology. To compare the present result with previously reported work, zinc oxide-silver (ZnO–Ag) and zinc oxide-gold (ZnO–Au) nanocomposites were prepared through wet chemical process and laced into single-walled carbon nanotubes (SWCNTs) to yield ZnO–Ag-SWCNTs and ZnO–Au-SWCNTs hybrids, which shows significant phagocytic and bactericidal activities against the Gram-negative bacteria *E. coli* and Gram-positive *S. aureus* which support the current antibacterial effect of ZnO NPs using plant extracts [33].

4. Conclusion

Synthesis of ZnO NPs from aqueous extracts of aerial parts of *R. multifidus* using green methods was confirmed by the formation of yellow precipitates. The synthesized NPs were characterized by using XRD, SEM, TGA-DTA, FTIR, and UV-DRS, and the result is consistent with previously reported articles for ZnO NPs. FTIR result shows the nitro compounds and aromatic amines as reducing and capping agents, while analysis of produced ZnO nanoparticles revealed a UV–vis absorption peak at 442 nm. XRD examination demonstrated that every diffraction peak matched the hexagonal wurtzite structure of ZnO NPs. ZnO NPs' spherical shape was confirmed by image taken using scanning electron microscopy. The synthesized ZnO NPs revealed a significant antibacterial activity against *E. coli*, *P. aeruginosa*, *S. aureus*, and *B. subtilis* relatively in all ratios. The significant phagocytic and bactericidal activities observed against the Gram-negative bacteria *E. coli* and Gram-positive *S. aureus* support the current antibacterial effect of ZnO NPs. The antiradical activities of produced ZnO NPs in various ratios show that plant material has the ability to scavenge free radicals. Generally, the present work indicates that there is a promising antibacterial and antioxidant nanoscale pharmaceutical product from *R. multifidus* aqueous aerial extracts using zinc metal and we strongly recommend testing more antifungal and anticancer activities of synthesized ZnO NPs in the future.

Data Availability

The data used to support the findings of this study are included within this article.

Conflicts of Interest

The authors declare that they have no conflicts of interest.

Acknowledgments

The authors are grateful to Adama Science and Technology University for the support rendered towards this work. We are also grateful to the World Academy of Sciences (TWAS) and the United Nations Educational, Scientific and Cultural Organization (UNESCO) for financing this research with funds allocated to the AD research team under the TWAS Research Grant RGA No. 20-274 RG/CHE/AF/AC_G – FR3240314163.

References

[1] M. O. Akpotu, P. M. Eze, C. C. Abba, C. U. Nwachukwu, F. B. C. Okoye, and C. O. Esimone, "Metabolites of endophytic fungi isolated from *Euphorbia hirta* growing in Southern Nigeria," *Chemical Science Review and Letters*, vol. 6, no. 21, pp. 12–19, 2017.

[2] A. B. Muluye, A. G. Desta, S. K. Abate, and G. T. Dano, "Antimalarial activity of the root extract of *Euphorbia abyssinica* (*Euphorbiaceae*) against *Plasmodium berghei* infection in mice," *Malaria Journal*, vol. 18, Article ID 261, 2019.

[3] F. Kaaniche, A. Hamed, A. S. Abdel-Razek et al., "Bioactive secondary metabolites from new endophytic fungus *Curvularia*. sp isolated from *Rauwolfia macrophylla*," *PLOS ONE*, vol. 14, no. 6, Article ID e0217627, 2019.

[4] B. Abebe, H. C. A. Murthy, and Y. Dessie, "Synthesis and characterization of Ti–Fe oxide nanomaterials: adsorption–degradation of methyl orange dye," *Arabian Journal for Science and Engineering*, vol. 45, pp. 4609–4620, 2020.

[5] M. G. Demissie, F. K. Sabir, G. D. Edossa, and B. A. Gonfa, "Synthesis of zinc oxide nanoparticles using leaf extract of *Lippia adoensis* (Koseret) and evaluation of its antibacterial activity," *Journal of Chemistry*, vol. 2020, Article ID 7459042, 9 pages, 2020.

[6] H. Jan, M. Shah, A. Andleeb et al., "Plant-based synthesis of zinc oxide nanoparticles (ZnO-NPs) using aqueous leaf extract of *Aquilegia pubiflora*: their antiproliferative activity against HepG2 cells inducing reactive oxygen species and other *in vitro* properties," *Oxidative Medicine and Cellular Longevity*, vol. 2021, Article ID 4786227, 14 pages, 2021.

[7] M. Naseer, U. Aslam, B. Khalid, and B. Chen, "Green route to synthesize zinc oxide nanoparticles using leaf extracts of *Cassia fistula* and *Melia azadarach* and their antibacterial potential," *Scientific Reports*, vol. 10, Article ID 9055, 2020.

[8] A. Raj and R. Lawerence, "Green synthesis and characterization of ZnO nanoparticles from leafs extracts of *Rosa indica* and its antibacterial activity," *RASĀYAN Journal of Chemistry*, vol. 11, no. 3, pp. 1339–1348, 2018.

[9] M. K. A. Mohammed, Z. J. Taqi, A. M. A. Hassen, M. S. Jabir, and D. S. Ahmed, "SWCNTs/ZnO-Ag/ZnO-Au nanocomposite increases bactericidal activity of phagocytic cells against *Staphylococcus aureus*," *AIP Conference Proceedings*, vol. 2372, no. 1, Article ID 020001, 2021.

[10] D. Zeleke, R. Eswaramoorthy, Z. Belay, and Y. Melaku, "Synthesis and antibacterial, antioxidant, and molecular docking analysis of some novel quinoline derivatives," *Journal of Chemistry*, vol. 2020, Article ID 1324096, 16 pages, 2020.

[11] W. Abebe, "An overview of ethiopian traditional medicinal plants used for cancer treatment," *European Journal of Medicinal Plants*, vol. 14, no. 4, pp. 1–16, 2016.

[12] M. Z. Bhatti, A. Ali, A. Ahmad, A. Saeed, and S. A. Malik, "Antioxidant and phytochemical analysis of *Ranunculus arvensis* L. extracts," *BMC Research Notes*, vol. 8, Article ID 279, 2015.

[13] M. S. Aslam, B. A. Choudhary, M. Uzair, and A. S. Ijaz, "The genus *Ranunculus*: a phytochemical and ethnopharmacological review," *International Journal of Pharmacy and Pharmaceutical Sciences*, vol. 4, no. 5, pp. 15–22, 2012.

[14] B. Madikizela, L. Kambizi, and L. J. McGaw, "An ethnobotanical survey of plants used traditionally to treat tuberculosis in the eastern region of O.R. Tambo district, South Africa," *South African Journal of Botany*, vol. 109, pp. 231–236, 2017.

[15] H. de Wet and S. C. Ngubane, "Traditional herbal remedies used by women in a rural community in northern Maputaland (South Africa) for the treatment of gynaecology and obstetric complaints," *South African Journal of Botany*, vol. 94, pp. 129–139, 2014.

[16] M. Giday, Z. Asfaw, Z. Woldu, and T. Teklehaymanot, "Medicinal plant knowledge of the bench ethnic group of Ethiopia: an ethnobotanical investigation," *Journal of Ethnobiology and Ethnomedicine*, vol. 5, Article ID 34, 2009.

[17] B. Sirak, L. Mann, A. Richter, K. Asres, and P. Imming, "In vivo antimalarial activity of leaf extracts and a major compound isolated from *Ranunculus multifidus* forsk," *Molecules*, vol. 26, no. 20, Article ID 6179, 2021.

[18] R. S. Devi and R. Gayathri, "Green synthesis of zinc oxide nanoparticles by using hibiscus rosa-sinensis," *International Journal of Current Engineering and Technology*, vol. 4, no. 4, pp. 2444–2446, 2014.

[19] K. Dulta, G. K. Ağçeli, P. Chauhan, R. Jasrotia, and P. K. Chauhan, "Ecofriendly synthesis of zinc oxide nanoparticles by *Carica papaya* leaf extract and their applications," *Journal of Cluster Science*, vol. 33, pp. 603–617, 2022.

[20] A. Kalbessa, A. Dekebo, H. Tesso, T. Abdo, N. Abdissa, and Y. Melaku, "Chemical constituents of root barks of *Gnidia involucrata* and evaluation for antibacterial and antioxidant activities," *Journal of Tropical Medicine*, vol. 2019, Article ID 8486214, 8 pages, 2019.

[21] T. Desalegn, H. C. A. Murthy, and Y. A. Adimasu, "Medicinal plant syzygium guineense (Willd.) DC leaf extract mediated green synthesis of Ag nanoparticles: investigation of their antibacterial activity," *Ethiopian Journal of Science and Sustainable Development*, vol. 8, no. 1, pp. 1–12, 2021.

[22] B. A. Lemecho, F. K. Sabir, D. M. Andoshe et al., "Biogenic synthesis of Cu-doped ZnO photocatalyst for the removal of organic dye," *Bioinorganic Chemistry and Applications*, vol. 2022, Article ID 8081494, 10 pages, 2022.

[23] A. A. Menazea, A. M. Ismail, and A. Samy, "Novel green synthesis of zinc oxide nanoparticles using orange waste and its thermal and antibacterial activity," *Journal of Inorganic and Organometallic Polymers and Materials*, vol. 31, pp. 4250–4259, 2021.

[24] E. F. El-Belely, M. M. S. Farag, H. A. Said et al., "Green synthesis of zinc oxide nanoparticles (ZnO-NPs) using *Arthrospira platensis* (class: cyanophyceae) and evaluation of their biomedical activities," *Nanomaterials*, vol. 11, no. 1, Article ID 95, 2021.

[25] M. Rafique, R. Tahir, S. S. A. Gillani et al., "Plant-mediated green synthesis of zinc oxide nanoparticles from *Syzygium Cumini* for seed germination and wastewater purification," *International Journal of Environmental Analytical Chemistry*, vol. 102, no. 1, pp. 23–38, 2022.

[26] E. T. Bekele, Y. D. Sintayehu, H. C. A. Murthy et al., "Synthesis of ZnO nanoparticles mediated by natural products of *Acanthus sennii* leaf extract for electrochemical sensing and photocatalytic applications: a comparative study of volume ratios," *Chemical Papers*, vol. 76, pp. 5967–5983, 2022.

[27] T. S. Aldeen, H. E. A. Mohamed, and M. Maaza, "ZnO nanoparticles prepared via a green synthesis approach: physical properties, photocatalytic and antibacterial activity," *Journal of Physics and Chemistry of Solids*, vol. 160, Article ID 110313, 2022.

[28] S. A. Wani, B. A. Khatoon, and F. Khanum, "Antioxidant catalytic and biological activities of zinc oxide nanoparticles synthesized by using lagerstreomia specio leaves," *International Journal of Innovations in Engineering Research and Technology*, vol. 8, no. 8, pp. 182–191, 2021.

[29] B. Abebe, E. A. Zereffa, and H. C. A. Murthy, "Synthesis of poly(vinyl alcohol)-aided ZnO/Mn_2O_3 nanocomposites for acid orange-8 dye degradation: mechanism and antibacterial activity," *ACS Omega*, vol. 6, no. 1, pp. 954–964, 2021.

[30] B. Abebe, H. C. A. Murthy, E. A. Zereffa, and Y. Adimasu, "Synthesis and characterization of ZnO/PVA nanocomposites for antibacterial and electrochemical applications," *Inorganic and Nano-Metal Chemistry*, vol. 51, no. 8, pp. 1127–1138, 2021.

[31] N. B. Raj, N. T. P. Gowda, O. S. Pooja et al., "Harnessing ZnO nanoparticles for antimicrobial and photocatalytic activities," *Journal of Photochemistry and Photobiology*, vol. 6, Article ID 100021, 2021.

[32] K. D. Dejen, E. A. Zereffa, H. C. A. Murthy, and A. Merga, "Synthesis of ZnO and ZnO/PVA nanocomposite using aqueous moringa oleifeira leaf extract template: antibacterial and electrochemical activities," *Reviews on Advanced Materials Science*, vol. 59, no. 1, pp. 464–476, 2020.

[33] O. Al Rugaie, M. S. Jabir, M. K. A. Mohammed et al., "Modification of SWCNTs with hybrid materials ZnO–Ag and ZnO–Au for enhancing bactericidal activity of phagocytic cells against *Escherichia coli* through NOX2 pathway," *Scientific Reports*, vol. 12, Article ID 17203, 2022.